ACS APPLIED MATERIALS & INTERFACES

Research Article

www.acsami.org

Effect of a Room-Temperature Ionic Liquid on the Structure and Properties of Electrospun Poly(vinylidene fluoride) Nanofibers

Chenyang Xing,[†,‡,§] Jipeng Guan,[†] Yongjin Li,*[,†] and Jingye Li*[,‡]

[†]College of Material, Chemistry and Chemical Engineering, Hangzhou Normal University, No. 16 Xuelin Rd., Hangzhou 310036, P. R. China

[‡]TMSR Research Center and CAS Key Lab of Nuclear Radiation and Nuclear Energy Technology, Shanghai Institute of Applied Physics, Chinese Academy of Sciences, Shanghai 201800, P. R. China

[§]University of Chinese Academy of Sciences, Beijing, 100049, P. R. China

Supporting Information

ABSTRACT: Novel anti-static nanofibers based on blends of poly(vinylidene fluoride) (PVDF) and a room-temperature ionic liquid (RTIL), 1-butyl-3-methylimidazolium hexafluorophosphate [BMIM][PF_6], were fabricated using an electrospinning approach. The effects of the RTIL on the morphology, crystal structure, and physical properties of the PVDF nanofibers were investigated. Incorporation of RTIL leads to an increase in the mean fiber diameter and the rough fiber surface of the PVDF/RTIL composite nanofibers compared with the neat PVDF nanofibers. The PVDF in the PVDF/RTIL nanofibers exhibits an extremely high content (almost 100%) of β crystals, in contrast to the dominance of PVDF γ crystals in bulk melt-blended PVDF/RTIL blends. Nonwoven fabrics produced from the electrospun PVDF/RTIL composite nanofibers show better stretchability and higher electrical conductivity than those made from neat PVDF without RTIL, and are thus excellent antielectrostatic fibrous materials. In addition, RTIL greatly improved the hydrophobicity of the PVDF fibers, enabling them to effectively separate a mixture of tetrachloromethane (CCl_4) and water. The extremely high β content, excellent antielectrostatic properties, better stretchability, and hydrophobicity of the present PVDF/RTIL nanofibers make them a promising candidate for micro- and nanoscale electronic device applications.

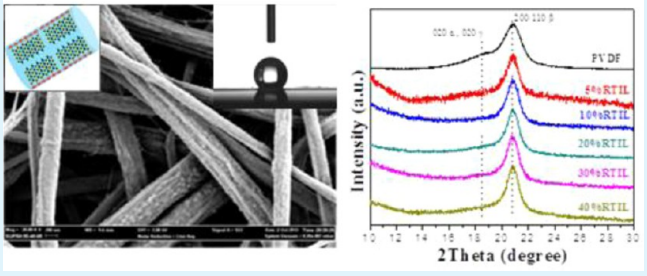

KEYWORDS: *poly(vinylidene fluoride), ionic liquid, nanofibers, crystals, electrospinning, conductivity*

1. INTRODUCTION

Poly(vinylidene fluoride) (PVDF), a versatile crystalline polymer, has drawn increasing attention in recent years becaues of its extraordinary properties including heat, abrasion, and chemical resistance, and good toughness, flexibility, weatherability, and particularly excellent electrical properties such as pizeo-, pyro-, and ferro-electricity.[1−13] PVDF is also notable for its polymorphism and is often observed in at least three regular conformations; namely, the all-trans (tttt) planar zigzag β-phase, the tg+tg− (trans gauche+ trans gauche−) α and δ phases, and the tttg+tttg- γ and ε phases.[14] Among these phases, the polar β and γ ones are the desirable crystal forms, especially the former, which has the largest spontaneous polarization (p) per unit cell and thus exhibits the highest pizeo-, pyro-, and ferroelectric activities. However, raw PVDF consists of the paraelectric α-phase. Many attempts have been made to suppress this nonpolar α-phase and enhance the content of the polar phases.[15−23] One of the effective approaches is the integration of nanofillers, especially those capable of providing high aspect ratio templates, such as montmorillonite[24,25] and carbon nanotubes (CNTs).[26−29] Ramasundaram et al. demonstrated that addition of organically modified montmorillonite (OMMT) into PVDF films resulted in formation of the β phase.[24] They also proposed an ion-dipole interaction model to illuminate the change in chain conformation of PVDF that occurs in the molten state (see Figure 1A). Moreover, the use of CNTs may also induce the emergence of the β phase with the help of external forces.[30] It has been proposed that the most energy-favorable configuration is adopted such that H atoms and CNTs surface are face-to-face (see Figure 1B).[29] However, poor compatibility made the pristine CNTs less effective in inducing the formation of β-PVDF. We have first found that the use of room temperature ionic liquid (RTIL) modified CNTs leads to significantly enhanced polar β crystal content with homogeneous CNT dispersion in the PVDF matrix.[16] Very recently, Nandi et al. found similar results.[31] We considered that layer-by-layer interactions among the CNT surface, RTIL cations, and the

Received: January 10, 2014
Accepted: March 5, 2014
Published: March 5, 2014

   dx.doi.org/10.1021/am500061v | ACS Appl. Mater. Interfaces 2014, 6, 4447−4457

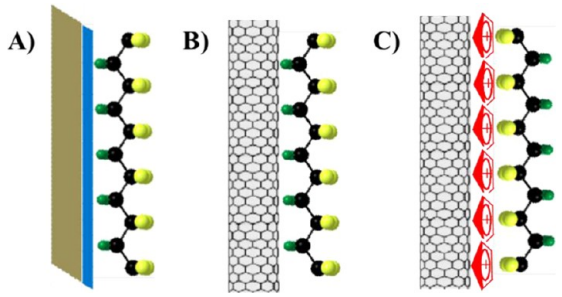

Figure 1. Typically schematic representation of formation for polar β-PVDF with the aid of the tangible templates of (A) OMMT,[24] (B) pristine CNTs,[29] and (C) ionic liquid modified CNTs.[16]

CF_2 groups of PVDF account for the formation of the polar β crystal form (see Figure 1C).[16] In view of these interesting phenomena, the corresponding possible mechanism of the formation of all-trans conformation PVDF using the aid of long tangible templates is proposed in Figure 1. OMMT[24] or modified CNTs,[16] with their intrinsic very large aspect ratio, are capable of interacting with the CH_2 (positive charge, δ^+) or CF_2 (negative charge, δ^-) groups of the PVDF, resulting in the large scale conformation of polar phases, especially the β ones. Other small molecular weight chemicals, including Ag nanoparticles,[32] metal salts,[33] and RTILs[34,35] have also been integrated into PVDF films to produce polar crystal forms. Although specific interactions between these fillers and PVDF matrix occur, the produced β-PVDF crystals do not dominate. This may be attributed to the fact that small (short) molecules cannot provide long enough sequences of tttt conformation of PVDF and that there were no templates to stabilize the high-energy tttt conformation.

Electrospinning has been demonstrated to be a facile technique to form the ferroelectric β phase of PVDF directly from polar solvents.[36−38] In electrospinning, a PVDF solution or melt is subjected to electrical poling and uniaxial stretching in a single step, which is helpful in overcoming the energy barrier of the molecular chain configuration and promote the formation of the polar β-crystals within the fibers. It has been further investigated that electrospinning combined with the addition of OMMT is an effective approach to generate a full content of all-trans β-PVDF.[39] This result is attributed to the creation of long trans-conformation chains by the electrospinning and the retardation of the relaxation of these extended chains by the OMMT platelets, which stabilized the conformation. Moreover, electrospinning with addition of magnetic nanoparticles[40] or electrospray deposition with addition of ionic fluorinated surfactant[41] are also capable of producing full polar β phase. Therefore, it is believed that combining electrospinning with an effective filler may be a more ideal route to obtain fiber-structured nonwoven composites with extremely high PVDF β phase content. Compared with their bulk or thin-film counterparts, piezoelectric PVDF composite nanofibers used as ultrathin fibers or membranes have greater potential for practical device applications.[42,43]

RTILs exhibit low toxicity, low melting points, negligible vapor pressure, high thermal and chemical stabilities, high ionic conductivity, and a broad electrochemical potential window.[44−46] In recent years, RTILs have not only been used as "green" organic solvents and safe electrolytes in solar cells, batteries, supercapacitors, and other electrochemical devices,[47−50] but have also been integrated into polymers to resolve the difficulties existing in their original matrice. For example, RTILs have been used as new generation plasticizers with higher efficiency and a lower bleeding (immigration of plasticizer) rate than traditional plasticizers. The effective plasticization of polymers using RTILs has been investigated for polyvinyl chloride (PVC),[51] poly(methyl methacrylate) (PMMA)[52,53] and PVDF.[35] Conversely, RTILs have also been found to be good compatibilizers for inorganic fillers and polymer matrices, enhancing their interfacial compatibility and the subsequent dispersion of fillers, especially for CNT[54−59] and montmorillonite[60] fillers. These compatibilizing effects are associated with interactions of the RTIL with both the polymers and the nanofillers. Even more interesting is that because of their high ionic conductivity, RTILs have also been applied as antistatic agents in polymers. Pernak et al. reported the antielectrostatic effects of imidazolium-based RTILs, and provided a reference to evaluate their antielectrostatic abilities.[61,62] Thus, integrating RTIL into a polymer matrix is an alternative way to resolve the problem of static-charge accumulation on the surface of a neat polymer because of its very high surface resistance (or volume resistance). Lu et al. reported the fabrication of a polystyrene (PS)/1-butyl-3-methylimidazolium hexafluorophosphate ([BMIM][PF_6]) nanofiber by electrospinning which exhibited superhydrophobicity and conductivity.[63] These properties were attributed to the intrinsic hydrophobicity and conductivity of [BMIM][PF_6]. It is believed that electrospun polymer/RTIL composite nanofibers have a large potential application in sensing materials; electrospun fibers with diameters ranging from several micrometers to nanometers have high specific surface area, which results in better sensing performance than that of the corresponding film forms. In addition, the integration of RTILs having high ionic mobility and ionic conductivity into electrospun fibers may enhance their electrical properties, which are also important for sensing materials. Kang et al. fabricated organic vapor sensors based on electrospun [BMIM][PF_6]/nylon 6,6 nanofiber and showed that their good sensing performance was owed to the incorporation of RTILs.[64]

In view of the unique characteristics of RTILs and the ferro- and piezoelectric features of PVDF, electrospun PVDF/RTIL composite nanofibers may be a promising candidate for micro- and nano-scale electronic devices such as sensors, actuators, energy generators and harvesters, as well as switches. However, to our best knowledge, no relevant study has been reported until now. In this paper, PVDF/RTIL composite nanofibers were prepared by electrospinning and the effect of RTIL on the structure and properties of the obtained nanofibers were investigated. The obtained composite nanofibers were found to exhibit extremely high polar β phase content, in contrast to the polar γ phase of the PVDF/RTIL films reported in our previous study.[35] More interestingly, the incorporation of RTIL into the PVDF nanofibers dramatically decreased their surface resistivity, making them an excellent antielectrical material. In addition, the resultant PVDF/RTIL nanofiber mats behaved as a good filter for tetrachloromethane (CCl_4)/water mixture separation.

2. EXPERIMENTAL SECTION

2.1. Materials and Sample Preparation. PVDF samples (trade name KF850) were supplied by Kureha Chemicals, Tokyo, Japan and were used as received. The molecular weight and polydispersity of the

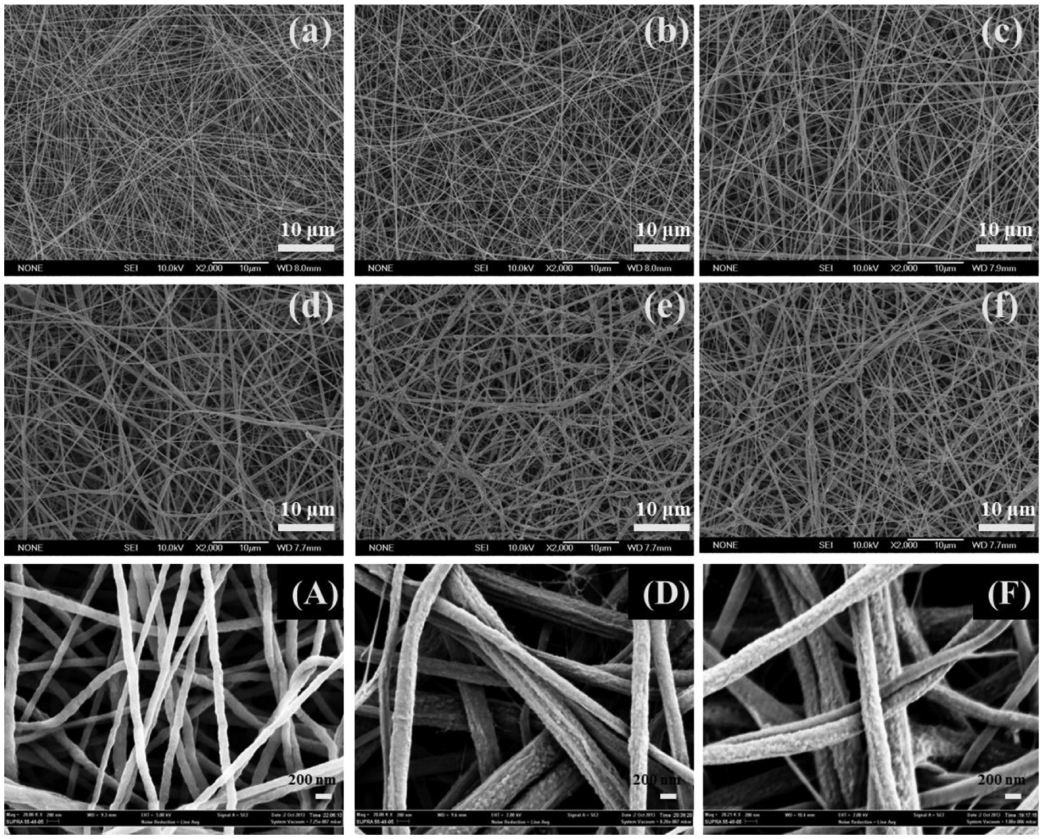

Figure 2. FESEM micrographs of electrospun PVDF and their composite nanofibers of PVDF/RTIL with different RTIL contents: (a, A) 0 wt % (neat PVDF); (b) 5 wt %; (c) 10 wt %; (d, D) 20 wt %; (e) 30 wt %; (f, F) 40 wt %, respectively. Note that micrographs of A, D, and F are high-resolution SEM images with the scale bar of 200 nm.

PVDF, determined by gel permeation chromatography, were M_w = 209,000 and M_w/M_n = 2.0, respectively. The RTIL 1-butyl-3-methylimidazolium hexafluorophosphate [BMIM][PF_6], was purchased from Aldrich and used as received. Dimethyl formamide (DMF) and acetone were employed as solvents for the PVDF.

First, a precursor solvent solution was prepared from DMF and acetone in a weight ratio of 6/4. PVDF/RTIL composites with different RTIL contents (0, 5, 10, 20, 30, and 40 wt %) were then added into the mixed solvent at a fixed solid/solvent ratio of 20 w/w%. The mixtures were stirred for 4 h at 70 °C until the PVDF pellets were fully dissolved and the solutions were then loaded into plastic syringes. The inside diameter of the needle at the end of the syringe was 0.25 mm. Electrospinning was conducted at 20 kV at a feed rate of 0.5 mL/h. The collector was a grounded and static plate covered with aluminum foil. The needle-to-collection plate distance was 15 cm. A nonwoven composite nanofiber mat was collected on the aluminum foil. All the electrospun nanofiber mats were dried in a vacuum at 75 °C overnight before characterization.

2.2. Sample Characterization. *Microstructure Investigation.* Field emission scanning electron microscopy (FESEM) was used to examine the surface morphology of the fiber samples (SEM-Zeiss Supra 55 Sapphira; Germany) and to determine the average diameter of the fibers (SEM-JSM 6700). The samples were sputter-coated with gold and examined at an acceleration voltage of 10 kV.

X-ray Photoelectron Spectroscopy (XPS) Analysis. XPS analysis was performed with a Kratos Axis Ultra instrument using monochromatic Al Kα radiation. Wide scans of the samples were carried out in the range 1100−0 eV, and narrow scans were performed for the N1s, P2p, F1s, and C1s regions.

Crystalline Structure Identification. The crystalline structures of all the fiber samples were studied by Fourier transform infrared spectroscopy (FTIR, Bruker Tensor) and X-ray diffraction (XRD, Bruker-D8). The FTIR spectra were recorded at a resolution of 2 cm^{-1}, and 16 scans from 4000 to 400 cm^{-1} were averaged. The FTIR measurements were carried out in transmittance mode on as-electrospun samples. The XRD data was collected from 2θ = 5−30° at a scanning speed of 2°/min with a step interval of 0.02°. The instrument was operated at 35 kV voltage and 30 mA current.

Thermal Behavior Study. The crystallization and melting behaviors of all samples were investigated by differential scanning calorimetry (DSC, TA-Q2000). Before each scan, the heat flow and temperature of the instrument were calibrated with sapphire and pure indium, respectively. The samples were first heated to 210 °C and held for 10 min to eliminate previous thermal history. The samples were then cooled to 20 °C, followed by heating again to 210 °C. Both the cooling and heating rates were 10 °C/min, and the experiments were conducted under a continuously flowing high purity nitrogen atmosphere. The first heating and cooling traces as well as the second heating traces were recorded.

Wettability Behavior. The contact angles of the samples were measured on a DSA100 machine (Data-Physics, Germany) at ambient temperature. Water and tetrachloromethane (CCl_4) droplets (DCE, about 4 μL) were dropped carefully onto the samples, and the average value of five measurements performed at different positions on each sample was adopted as the contact angle.

Separation of a Mixture. The PVDF/RTIL composite nanofiber sample with 20 wt % RTIL loading was used to separate a mixture of tetrachloromethane (CCl_4) and water (4/1, v/v) under normal atmospheric pressure. Water in the CCl_4 was easily detected using a polarized optical microscope (POM, Olympus BX51-P).

Electrical Properties. The electrical conductivity of the samples was measured using an ultrahigh-resistivity meter with a URS probe electrode (model MCP-HT450) at a voltage of 10 V. A ring electrode probe consisting of an inner electrode and outer electrode was directly placed on the samples for the measurements. At least five different

locations on each sample were measured and the average value was used.

Mechanical Properties. Tensile tests were carried out using an Instron universal material testing system (model 5966) at 23 °C, with a gauge length of 18 mm and crosshead speed of 10 mm/min. Dumbbell shaped samples were directly punched out from the electrospun fiber mats. Five samples were tested and averaged for each formulation.

3. RESULTS AND DISCUSSION

3.1. Morphology of the PVDF/IL Composite Nanofibers. We have previously reported the effects of RTIL addition on the structure and properties of PVDF in bulk melt-blended PVDF/RTIL blends.[35] RTIL exhibits drastic effects on both the crystal forms and physical properties of PVDF in the bulk state. It is therefore interesting to investigate the effects of RTIL on the structure and properties of electrospun PVDF nanofibers. Figure 2 shows SEM images of neat PVDF and PVDF/RTIL composite nanofibers electrospun from corresponding solutions in DMF/acetone which contained different amounts of RTIL. Detailed information on the fabricated nanofibers, including the dependences of the fiber diameter and diameter distribution on the RTIL loading is shown in Figure 3

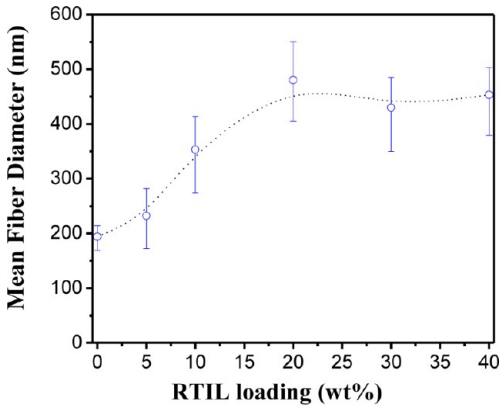

Figure 3. Plot of mean fiber diameter vs. RTIL loadings for electrospun PVDF and PVDF/RTIL composite nanofibers.

and Figure S1 in the Supporting Information. The fibers produced from the neat PVDF were observed to be uniform in diameter except for a few small irregular beads placed along the fibers. These beads had diameters varying between 500 and 750 nm (see Figure 2a). The mean fiber diameter was calculated to be around 194 ± 40 nm. It can also be seen that all of the neat PVDF fibers had smooth surfaces (see Figure 2A), indicating almost full evaporation of the solvent in the nanofibers before the fibers were deposited onto the collector. With increasing RTIL loading, the irregular beads along the fibers disappeared but the diameters of the nanofibers as well as their distribution became much larger and wider compared with that of neat PVDF fiber, as shown in Figure 3. In addition, the surfaces of the PVDF/RTIL fibers were much rougher than that of neat PVDF, as seen in the images of composite fibers with RTIL loadings of 20 and 40 wt % (Figure 2D, F, respectively). Although RTIL exhibits clear effects on both the fiber diameter and fiber surface of the final PVDF/RTIL nanofibers, no drastic difference was observed in terms of the macroscopic appearance of the fiber mats, as seen in Figure S2 in the Supporting Information. It should be noted that the amount of RTIL incorporated into the nanofibers was the same as the feeding ratio in the precursor solution, as evidenced by the almost identical FTIR spectra of the precursor solution and the films produced from the dissolved nanofiber solution.

It is well known that the morphologies of nanofibers fabricated by electrospinning are highly dependent on the electrospinning solution properties, such as conductivity, viscosity, and surface tension. The addition of RTIL or other salts into the polymer solution is capable of increasing solution conductivity gradually, while other solution parameters including viscosity and surface tension show more complex changes.[65,66] The solution conductivities of the PVDF/RTIL solutions used in the present work were largely increased by the ion-conductive RTIL molecules, which may have facilitated fiber aggregation and fusion. The fiber extension process continuously occurs before fiber solidification or deposition. Therefore, the mean diameter of the PVDF/RTIL fibers was increased with a broad varying range. The increased degree of surface roughness of the composite fiber may be attributed to relatively slow evaporation of the mixed solvent. This is because the mixed solvent, added RTIL, and PVDF matrix interacted with each other in solution, which consequently hindered immediate evaporation of the solvent and led to a much rougher fiber surface. Other authors have reported the same phenomenon and explained it by the existence of small RTIL crystals.[67] However, the RTIL [BMIM][PF_6] used in this work crystallizes upon heating at around −37 °C and melts at around 11 °C, both of which are far lower than room temperature.[68] Thus, the possible existence of small RTIL crystals on the surface of PVDF/RTIL fibers was not taken into account as the reason for such a rough surface of the PVDF/RTIL fibers.

Figure 4 shows the XPS spectra of neat PVDF and PVDF/RTIL composite nanofibers with RTIL loadings of 5, 20, and 40 wt %. As shown in Figure 4a−c, the existence of N (N1s, at 401.7 eV) and P (P2p, at 136.2 eV) element signals indicates that the RTIL was present on the surface of the PVDF/RTIL composite nanofiber.[69] It can be seen that both the F1s and C1s of XPS core-level scan spectra have a decreased binding energy (BE), compared neat PVDF fiber with the PVDF/IL composie nanofibers. This indicates their electron cloud density has changed under the specific interaction between PVDF and RTIL molecules. On the other hand, it can also be seen that the BE of N1s and P2p were slightly decreases with the addition of RTIL. Obviously, the shifts confirm the interaction between PVDF and RTIL molecules, which is consistent with the results previously reported.[35] Note that much smaller shifts for the N1s and P2 than F1s was observed, which can be attributed to the delocalization of imidazulium ring upon the interaction with PVDF molecular chains.

3.2. Crystalline Structure. The crystalline structure of the electrospun fibers was determined using X-ray diffraction (XRD) and Fourier transform infrared (FTIR) spectroscopy. Figure 5 shows XRD patterns of the neat PVDF and its composite nanofibers containing different amounts of RTIL. The neat PVDF electrospun nanofibers showed a distinctive X-ray diffraction peak at 20.9° which is indexed to β (200/110) reflections for the crystalline PVDF conformation.[15,70] A broad shoulder was also observed at about 18.4−18.6°, which corresponds to the (020) reflection of the nonpolar α phase. However, it is reported that the α (020) crystal plane peak frequently overlaps the γ (020) one and the amorphous halo of PVDF.[25,71] Therefore, the γ phase cannot be precisely identified from the α phase and amorphous halo of the neat PVDF electrospun nanofiber using only the X-ray scattering

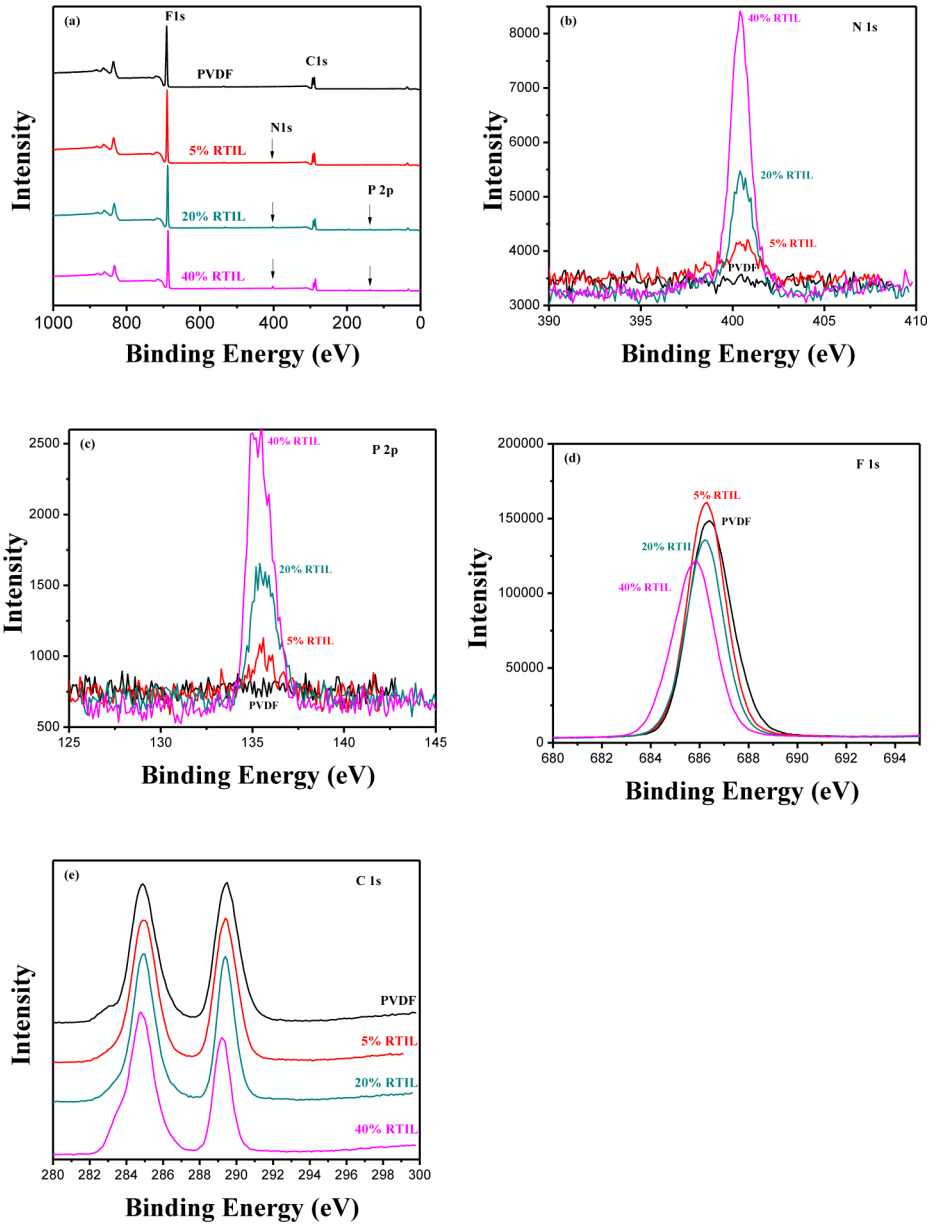

Figure 4. (a) XPS wide scan spectra and (b–e) element core-level spectra of neat PVDF and PVDF/RTIL composite nanofibers with the RTIL loadings of 5, 20, and 40%, respectively.

data. The following FTIR data (Fig. 6a) indicates that only β and γ phases coexisted in this sample, so it can be concluded that the diffraction at about 18.4–18.6° originated from the γ phase. As RTIL was added, the broad shoulder diffraction diminished and only the diffraction peak of the PVDF β crystals was observed. This indicates that the incorporation of RTIL was capable of facilitating the conformation of all-trans β crystal under electrospinning. This phenomenon is of great interest because small molecule RTILs are more favorable to induce not only the long sequence of β phase but the short sequence of γ-PVDF crystallized from the molten state, as shown in our previous study,[35] owing to the lack of a template to stabilize the higher energy tttt conformation of PVDF. Thus, in the case of melt-crystallized PVDF/RTIL films, the γ phase is dominantly crystallized because of the specific interaction between PVDF and RTIL.[16,35] However, a totally different situation occurs for PVDF/RTIL nanofibers formed by electrospinning. During the process of electrospinning, the PVDF molecular chains are uniaxially stretched by high electrical forces, resulting in orientation of the dipoles of PVDF (CF_2 or CH_2 dipoles). Additionally, along with the specific interaction of the imidazolium ions of the RTIL with CF_2, the long tttt conformation PVDF chains were further stabilized and large amounts of β crystal were obtained. To date, we can easily control the dominant β or γ crystalline type of PVDF through the use of RTIL, not only in film-structured[16,35] but also in fiber-structured composites, which is of great importance for diverse application of ferro- and piezoelectric PVDF.

To further identify the crystal structures present in the electrospun PVDF fibers, FTIR measurements were carried out on all samples, as shown in Figure 6a. The bands at 445 and 1275 cm^{-1} correspond to the all-trans conformation of the β phase, and the band at 1234 cm^{-1} is assigned to the tttg conformation of the γ phase.[72−74] It is reported that the band at 840 cm^{-1} is the absorbance of trans chains longer than tt, which is produced in both the β and γ phase.[25,71] From the FTIR

dx.doi.org/10.1021/am500061v | ACS Appl. Mater. Interfaces 2014, 6, 4447−4457

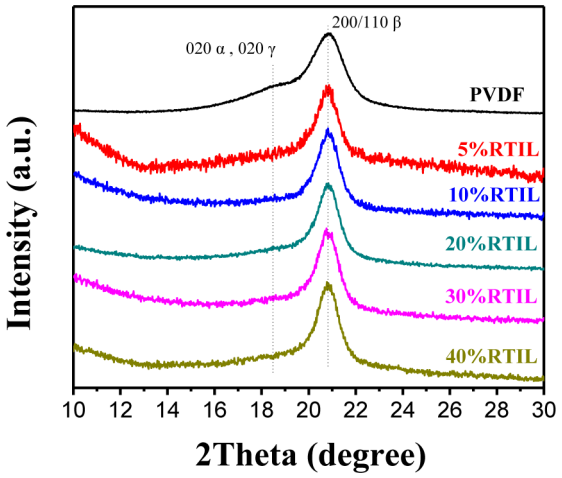

Figure 5. Room-temperature wide-angle X-ray scattering intensity (λ = 0.1542 nm) vs. scattering angle, two theta, for electrospun PVDF and PVDF/RTIL composite nanofiber, at the RTIL compositions indicated.

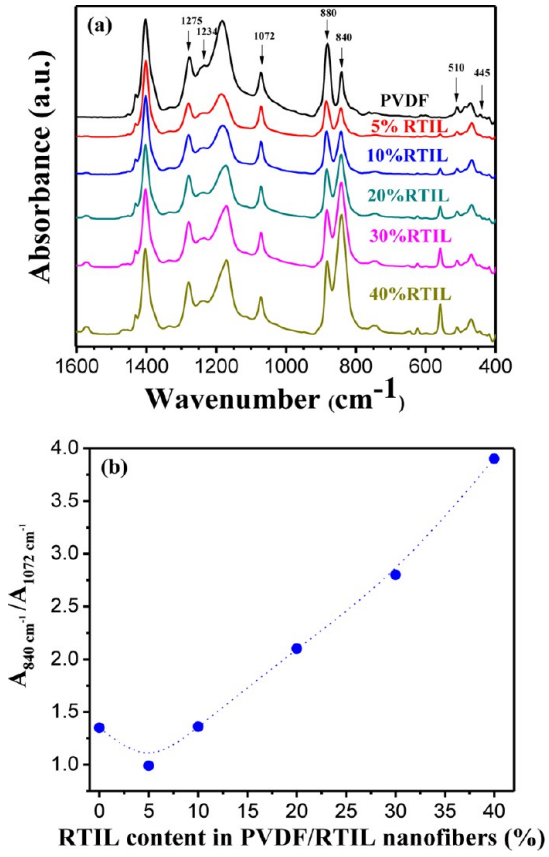

Figure 6. (a) FTIR absorbance vs. wavenumber and (b) plot of $A_{840\ (cm^{-1})}/A_{1072(cm^{-1})}$ vs. RTIL content for electrospun PVDF and PVDF/RTIL composite nanofibers.

spectra, one can see that no characteristic absorptions of nonpolar α phase were observed in the neat PVDF electrospun nanofiber. Furthermore, the clear absorptions at 445, 510, 840, 1234, and 1275 cm^{-1} indicated that β co-existed with the γ phase in all of the samples. Combining this data with the X-ray scattering results, it can be concluded that a very high content of β phase was obtained in the electrospun PVDF nanofibers. The absorption intensity of the band at 840 cm^{-1} significantly increased with RTIL content in the PVDF/RTIL composite nanofibers. This means that the content of polar crystal phases (β and γ) was greatly enhanced by the addition of RTIL. To quantitatively evaluate the PVDF polar crystal phase content in the composite nanofibers, the band at 1072 cm^{-1} was selected as a reference, which was regarded as only proportional to the sample thickness.[75] The area of the absorption at 840 cm^{-1} with respect to the reference band is plotted as a function of RTIL content in Figure 6b. The relative content of polar crystal phases (almost only β crystals) first exhibited a small drop at an RTIL content of 5% and then gradually increased with the RTIL content. Note that the content of γ phase was rather small, as shown by the XRD results, and that the enhanced amount of polar phase was therefore largely attributed to the increased β phase. We also note that absorption intensity of the band at 880 cm^{-1}, which is assigned to the amorphous peak of CF_2-CH_2 bending vibration,[76,77] also exhibited evident change when RTIL was added, showing that the conformation of molecules in the amorphous region of PVDF was also influenced by the electrospinning.

On the basis of the above XRD, XPS, and FTIR results, a proposed schematic for the PVDF/RTIL composite nanofibers is shown in Figure 7. During the process of electrospinning, the

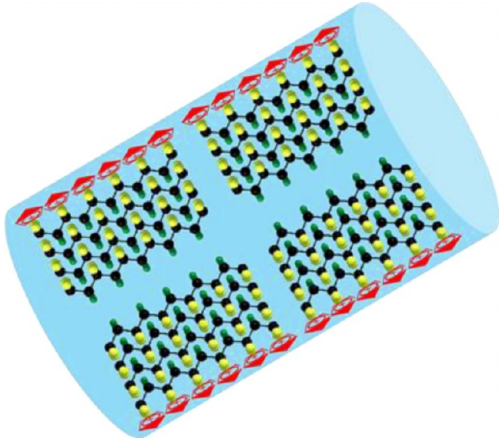

Figure 7. Schematic showing the proposed mechanism about the formation of β crystal phase in the electrospun PVDF/RTIL composites fibers, where the red rings arranged on the surface of the fiber denote the imidazolium ions and balls with the yellow, green, and black colors are the atoms of F, H, and C element in PVDF, respectively. And particularly, CF_2 group (negatively charged) could interact with the imidazolium ions (positively charged) of RTIL by the static interaction.

PVDF molecular chains were uniaxially stretched by high electrical forces, resulting in orientation of the dipoles of the PVDF (CF_2 or CH_2 dipoles). This "fictitious template" flow field caused by the electrical poling and uniaxial stretching of the polymer solution is rather similar to tangible templates such as OMMT and CNTs (shown in Figure 1), and led to the effective formation of a β-PVDF all-trans conformation. However, the just ejected extended molecules of PVDF that were a very close distance from the needle were still in the solution state, and their relaxation probably caused the transformation of the high energy and unstable tttt configuration of the β phase to the tttg+tttg− configuration of the γ phase. As a result, the neat PVDF fiber exhibited a large amount of β phase but little γ phase. It is very interesting that the specific interaction between the imidazolium ions of the

RTIL and the CF_2 groups of the PVDF was able to stabilize the unstable β phase configuration and hinder the possible transformation to the γ phase. Once the β-PVDF nuclei appeared as the solvents evaporated, β crystals of PVDF were substantially formed during the crystallization. As a result, almost 100% β phase was obtained. Additionally, the rougher surface of the PVDF/RTIL fibers (Figure 2), probably caused by the RTIL slowing the evaporation of the mixed solvent, and the existence of the N 1s and P 2p signals in the XPS results point to the likelihood that some RTIL molecules may have been located on the surface of the PVDF/RTIL fibers.

3.3. Thermal Behaviors. Figure 8a shows DSC heating curves for the PVDF/RTIL composite nanofibers with different amounts of RTIL incorporation. Double melting peaks were observed for all of the samples. However, only one melting peak, close to the higher melting peak temperature, was obtained when all the samples were subjected to a second heating run (see Figure 8c). This means that the lower melting peak originated from the melting of the ordered structure formed during the electrospinning. In other words, the electrospinning of the PVDF/RTIL composites induced the ordered (oriented) structure in addition to the formation of PVDF crystals. The disruption of the ordered structure during heating led to endothermic effects, which corresponds to the lower melting peak. This thermal behavior corresponds well to the decreased absorption intensity of the PVDF amorphous region at 880 cm^{-1}. In fact, such phenomena have been reported in many previous reports on oriented semicrystalline polymers.[78] The endothermic peak at high temperature is attributed to the melting of the β crystal phase in the nanofibers. We have reported that PVDF and RTIL are thermodynamically miscible, which induces depression of not only the melting temperature (T_m) but also the crystallization temperature (T_c).[35] In the present work, the composite nanofibers with RTIL also showed depression of both T_m and T_c (see Figure 8a, b) compared with the nanofibers without RTIL, indicating again the specific interaction between PVDF and RTIL.

3.4. Physical Properties. *Wettability Behavior.* The marked change in morphology of the electrospun PVDF fibers had significant influence on their wettability behavior, as shown in Figure 9. The electrospun PVDF fibers exhibited a water contact angle (WCA) of 140°, whereas the neat PVDF-film fabricated by melt-blending showed a WCA of only 90°. The WCA of the PVDF/RTIL composite nanofibers initially gradually increased with RTIL incorporation. The maximum WCA was about 147° for the sample with 20 wt.% RTIL. This increase in WCA was caused by the increased surface roughness of the electrospun PVDF/RTIL composite nanofibers compared with that of the neat PVDF fibers. The intrinsic hydrophobic properties of the RTIL could also have been responsible. As the RTIL content was further increased, the WCA value leveled off, as shown in Figure 9h. Moreover, the PVDF/RTIL fibers also showed good oleophilic properties, as seen in Video 1 in the Supporting Information. Because of its good hydrophobicity and oleophilicity, the PVDF/RTIL fiber with 20 wt % RTIL loading showed good separation of a mixture of tetrachloromethane (CCl_4) and water, as shown in Figure 10 and Video 2 in the Supporting Information. In the optical microscopy images, irregular water domains with diameters varying from 2 to 10 μm were clearly observed before separation (see Figure 10A), whereas no water domains were seen after separation of the mixture. The concentration of

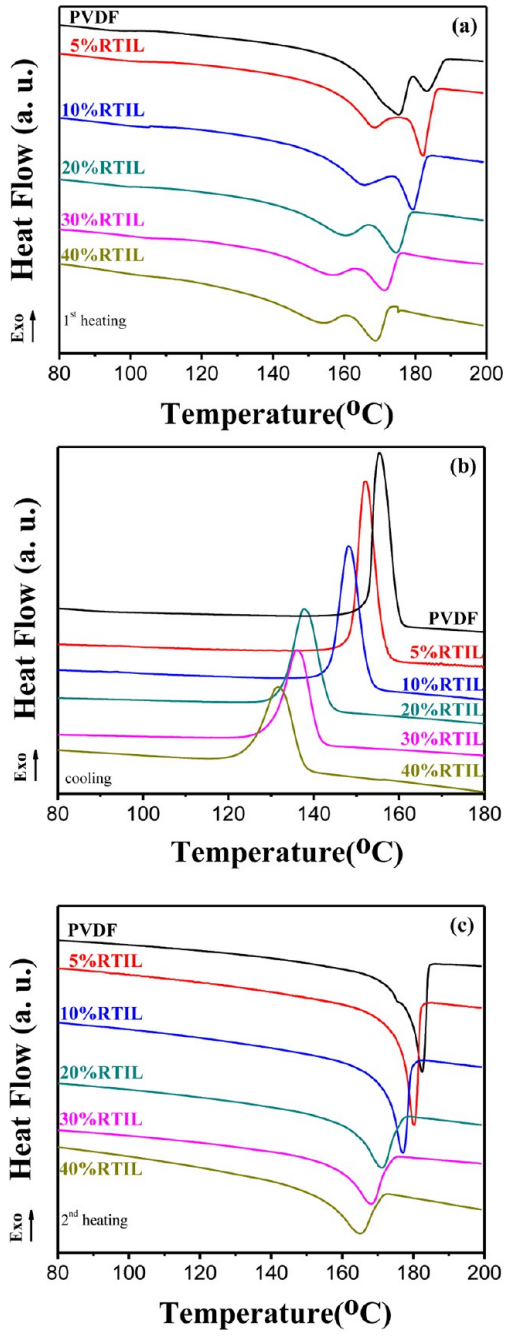

Figure 8. DSC scans showing (a) the first melting endotherms of electrospun PVDF and PVDF/RTIL composite nanofibers; (b) the follow-up crystallization of the samples from a molten state; (c) the follow-up second melting endotherms of these samples. And the heating (cooling) rate was always 10 °C/min.

water in the CCl_4 after the separation was evaluated to be as low as 45.6 ppm, which is slightly lower than the 48.2 ppm obtained using the neat PVDF nanofibers. This slight increase in separation efficiency may be ascribed to the increase in hydrophobicity of PVDF nanofibers by the addition of RTIL. These results indicate that nonwoven fibrous membranes fabricated from PVDF/RTIL composite nanofibers are potentially applicable to heavy oil/water separation. The separation efficiency is very high. Detailed investigation on the application of our fibrous materials to separation will be reported elsewhere. Note that no RTIL bleeding was observed

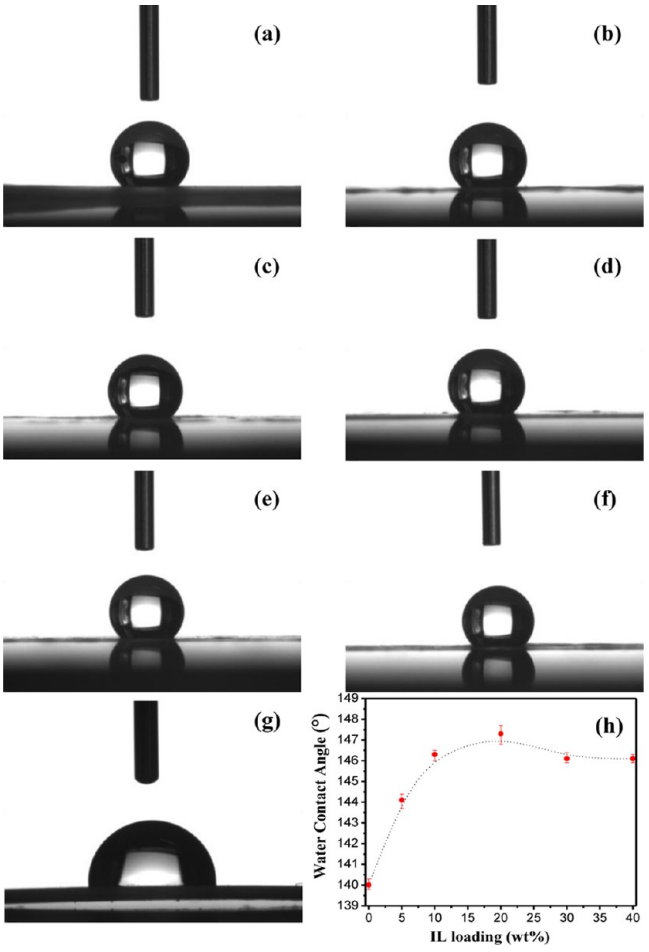

Figure 9. Photographs of a water droplet on (a) the as-prepared electrospun PVDF and (b–f) PVDF/RTIL composite nanofibers with the RTIL content of (b) 5, (c) 10, (d) 20, (e) 30, and (f) 40%; (h) a plot of water contact angle (WCA) of all electrospun fibers as a function of RTIL content, in which the average value of five measurements performed at different positions on the same samples was adopted as the WCA. (g) As a comparison, the neat PVDF-film melt-blended was also measured with the same condition.

when the nonwoven membrane was exposed to the CCl_4/H_2O mixture because of the strong interaction between the PVDF and the RTIL.

Electrical Properties. Because of their high ionic conductivity and easy processability in a liquid state, RTILs are also incorporated into polymers to eliminate the accumulation of static charges. Fiber materials with excellent antielectrostatic performance are often avoided by the adsorption of charges, bacteria as well as dusty in air, which could assure stable properties of materials in the practical use. Table 1 and Figure

Table 1. Electrical Conductivity of Neat PVDF and the PVDF/RTIL Composite Nanofiber with Different RTIL Loadings

fiber samples	surface resistivity (Ω /□)	volume resistivity (Ω cm)
neat PVDF	over range	over range
PVDF/RTIL (5 wt.%)	5.43×10^{11}	5.38×10^{10}
PVDF/RTIL (10 wt.%)	2.37×10^{10}	2.32×10^{9}
PVDF/RTIL (20 wt.%)	1.02×10^{9}	1.01×10^{8}
PVDF/RTIL (30 wt.%)	2.14×10^{8}	2.12×10^{7}
PVDF/RTIL (40 wt.%)	7.32×10^{7}	7.26×10^{6}

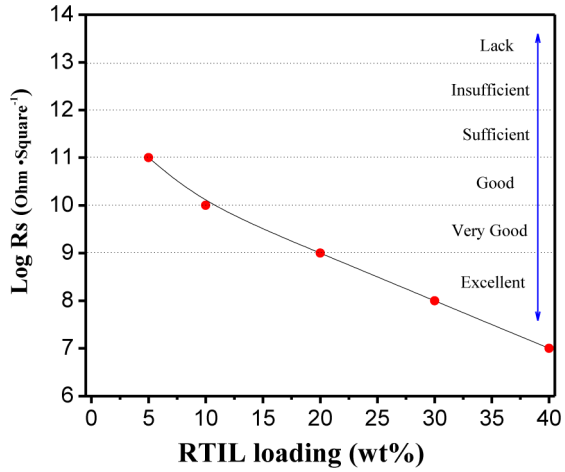

Figure 11. Plot of surface resistivity (R_s) vs. RTIL loading for electrospun PVDF and PVDF/RTIL composite nanofibers. The evaluation of antielectrostatic ability for each sample was judged from refs 61 and 62.

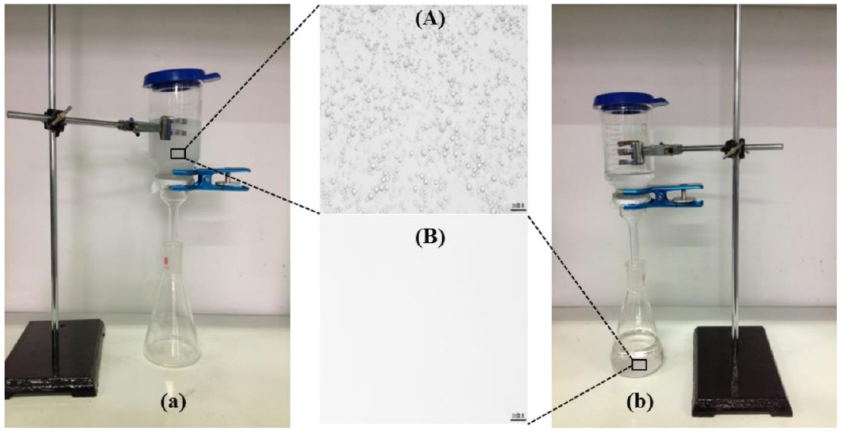

Figure 10. Photographs of (a, A) before and (b, B) after separation for a mixture of tetrachloromethane (CCl_4) and water for PVDF/RTIL fibers with 20 wt % RTIL loading (see Figure S3 in the Supporting Information). Images A and B are obtained from POM with the scale bar of 20 μm.

11 show the electric conductivity and antielectrostatic effects, respectively, of neat PVDF and PVDF/RTIL composite nanofibers with different RTIL loadings. Neat PVDF nanofiber lacked an antielectrostatic effect owing to its very poor electric charge, not detectable in our measurements. Incorporation of RTIL into the PVDF nanofibers effectively decreased the two types of resistivity. The antielectrostatic effects varied from "none" for PVDF to "good" and "excellent" for PVDF/RTIL composite nanofibers with the RTIL loadings of 10 and 20%, respectively. We also noted that the antielectrostatic effect of the as-prepared fiber samples was slightly weaker than that of the PVDF/RTIL films obtained by melt-blending for the same loading of RTIL. This may be because of the fiber-structured PVDF/RTIL samples, which had a large porosity, having few conductive paths of RTIL compared with the compacted melt-blended PVDF/RTIL films.

Mechanical Properties. The modulus of an individual electrospun nanofiber segment can be evaluated by atomic force microscopy (AFM), although the corresponding tensile strength and elongation at the break of a single nanofiber have not been obtainable.[79] In our study, the traditional strain−stress mode measured by stretching test was used to evaluate the average mechanical properties of the PVDF/RTIL composite nanofibers. Typical strain−stress curves of the neat PVDF fiber sheet and the PVDF/RTIL composite fiber sheet with an RTIL loading of 20% are presented in Figure 12. As can be seen,

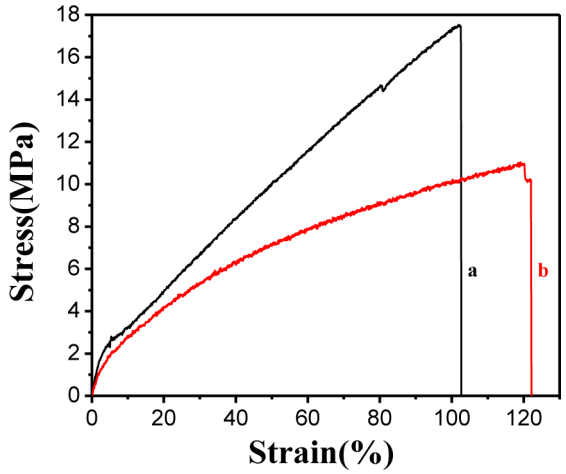

Figure 12. Stress−strain curves of (a) neat PVDF fiber mat and (b) PVDF/RTIL composite fiber mat with the RTIL loading of 20%. The measured fiber mats with uniform thickness are directly obtained from the aluminum foil collector. All this measurement was performed 5 times at room temperature.

addition of RTIL decreased the tensile strength from 17.5 MPa for the neat PVDF fiber sheet to 10.9 MPa. However, the elongation at break was increased by the RTIL addition, from 102% for the neat PVDF fiber sheet to 120%. This may be largely attributed to the plasticization effect of RTIL causing increased stretchability and ductility of the PVDF. In addition, as the schematic of the PVDF/RTIL composite fiber shows (see Figure 7), the RTIL molecules existing on the fiber surface may have produced weak interactions between the nanofibers in the sheet by a lubrication effect, which was also responsible for the improved stretchability.

4. CONCLUSIONS

In this work, PVDF/RTIL composite nanofibers were prepared from DMF/acetone solutions by electrospinning, and the morphology, crystalline structure, and physical properties of the as-obtained PVDF fibers were carefully investigated. Addition of RTIL caused an increase in solution conductivity, resulting in an increase in the mean fiber diameter and its standard deviation. Moreover, the surface of the PVDF/RTIL composite fibers became much rougher owing to the RTIL causing slower evaporation of the mixed solvent. From the XPS results, it was found that some RTIL molecules were located on the surface of PVDF/RTIL fibers but not in the form of RTIL crystals. The PVDF/RTIL composite nanofibers exhibited extremely high contents (almost 100%) of the all trans β crystal form, which distinctly differs from the dominant γ phases observed for melt-blended PVDF/RTIL blends.[35] The integration of RTIL into the PVDF fiber largely increased the electrical conductivity of the PVDF fibers, making an excellent antielectrostatic nanofibrous material. Meanwhile, the as-prepared composite nanofiber mats showed better stretchability and hydrophobicity than the neat PVDF mats, and exhibited good separation of a mixture of CCl_4 and water. Thus, new multifunctional PVDF/RTIL composite nanofibrous materials with extremely high polar β phase content and excellent antielectrostatic properties as well as stretchability and hydrophobicity were successfully obtained by electrospinning. These materials may be promising candidates for micro- and nanoscale electronic device applications.

■ ASSOCIATED CONTENT

Ⓢ Supporting Information

Data of fiber diameter distribution, and photo and relevant videos for PVDF/RTIL nanofibers. This material is available free of charge via the Internet at http://pubs.acs.org/.

■ AUTHOR INFORMATION

Corresponding Authors

*E-mail: yongjin-li@hznu.edu.cn. Tel: 86-571-2886-7206. Fax: 86-571-2886-7899.

*E-mail: jingyeli@sinap.ac.cn

Notes

The authors declare no competing financial interest.

■ ACKNOWLEDGMENTS

This work was financially supported by the National Natural Science Foundation of China (51173036, 21374027), PCSIRT (IRT 1231), and Program for New Century Excellent Talents in University.

■ REFERENCES

(1) Yu, W. X.; Zhao, Z. D.; Zheng, W. T.; Song, Y. M.; Li, B.; Long, B. H.; Jiang, Q. Structural Characteristics of Poly (Vinylidene Fluoride)/Clay Nanocomposites. *Mater. Lett.* **2008**, *62*, 747−750.

(2) Vo, L. T.; Giannelis, E. P. Compatibilizing Poly (Vinylidene Fluoride)/Nylon-6 Blends with Nanoclay. *Macromolecules* **2007**, *40*, 8271−8276.

(3) Li, Y. J.; Kaito, A.; Horiuchi, S. Biaxially Oriented Lamellar Morphology Formed by the Confined Crystallization of Poly (1, 4-Butylene Succinate) in the Oriented Blend with Poly (Vinylidene Fluoride). *Macromolecules* **2004**, *37*, 2119−2127.

(4) Wang, M.; Shi, J. H.; Pramoda, K. P.; Gol, S. H. Microstructure, Crystallization and Dynamic Mechanical Behaviour of Poly (Vinylidene Fluoride) Composites Containing Poly (Methyl Methacrylate)-

Grafted Multiwalled Carbon Nanotubes. *Nanotechnology* **2007**, *18*, 235701.
(5) Li, Y. J.; Iwakura, Y.; Zhao, L.; Shimizu, H. Nanostructured Poly (Vinylidene Fluoride) Materials by Melt Blending with Several Percent of Acrylic Rubber. *Macromolecules* **2008**, *41*, 3120−3124.
(6) Li, Y. J.; Iwakura, Y.; Shimizu, H. Polymer Crystallites with Few Tie Molecules from A Miscible Polymer Blend. *Macromolecules* **2008**, *41*, 3396−3400.
(7) Nam, Y. W.; Kim, W. N.; Cho, Y. H.; Chae, D. W.; Kim, G. H.; Hong, S. P.; Hwang, S. S.; Hong, S. M. Morphology and Physical Properties of Binary Blend Based on PVDF and Multi-Walled Carbon Nanotube. *Macromol. Symp.* **2007**, *249-250*, 478−484.
(8) Chen, D.; Wang, M.; Zhang, W. D.; Liu, T. X. Preparation and Characterization of Poly (Vinylidene Fluoride) Nanocomposites Containing Multiwalled Carbon Nanotubes. *J. Appl. Polym. Sci.* **2009**, *113*, 644−650.
(9) Qiu, Z.; Yan, C.; Lu, J.; Yang, W.; Ikehara, T.; Nishi, T. Various Crystalline Morphology of Poly(butylene Succinate-co-butylene Adipate) in Its Miscible Blends with Poly(vinylidene Fluoride). *J. Phys. Chem. B* **2007**, *111*, 2783−2789.
(10) Nishi, T.; Wang, T. T. Melting Point Depression and Kinetic Effects of Cooling on Crystallization in Poly (Vinylidene Fluoride)-Poly (Methyl Methacrylate) Mixtures. *Macromolecules* **1975**, *8*, 909−915.
(11) Vidhate, S.; Shaito, A.; Chung, J.; Dsouza, N. A. Crystallization, Mechanical, and Rheological Behavior of Polyvinylidene Fluoride/Carbon Nanofiber Composites. *J. Appl. Polym. Sci.* **2009**, *112*, 254−260.
(12) Li, Y. J.; Shimizu, H. Conductive PVDF/PA6/CNTs Nanocomposites Fabricated by Dual Formation of Cocontinuous and Nanodispersion Structures. *Macromolecules* **2008**, *41*, 5339−5344.
(13) Chang, C.; Tran, V. H.; Wang, J.; Fuh, Y. K.; Lin, L. Direct-Write Piezoelectric Polymeric Nanogenerator with High Energy Conversion Efficiency. *Nano Lett.* **2010**, *10*, 726−731.
(14) Lovinger, A. J. Ferroelectric Polymers. *Science* **1983**, *220*, 1115−1121.
(15) Czerw, N. R.; Xing, S. Y.; Iyer, P.; Carroll, D. L. Properties of Polyvinylidene Difluoride-Carbon Nanotube Blends. *Nano Lett.* **2004**, *4*, 1267−1271.
(16) Xing, C. Y.; Zhao, L. P.; You, J. C.; Dong, W. Y.; Cao, X. J.; Li, Y. J. Impact of Ionic Liquid-Modified Multiwalled Carbon Nanotubes on the Crystallization Behavior of Poly (Vinylidene Fluoride). *J. Phys. Chem. B* **2012**, *116*, 8312−8320.
(17) Zhao, Z. D.; Zheng, W. T.; Yu, W. X.; Long, B. H. Direct and Large Scale Electric Arc Discharge Synthesis of Boron and Nitrogen Doped Single-Walled Carbon Nanotubes and Their Electronic Properties. *Carbon* **2009**, *47*, 2112−2115.
(18) Wang, M.; Shi, J. H.; Pramoda, K. P.; Goh, S. H. Microstructure, Crystallization and Dynamic Mechanical Behaviour of Poly (Vinylidene Fluoride) Composites Containing Poly (Methyl Methacrylate)-Grafted Multiwalled Carbon Nanotubes. *Nanotechnology* **2007**, *18*, 235701.
(19) Mandal, A.; Nandi, A. K. Physical Properties of Poly (Vinylidene Fluoride) Composites with Polymer Functionalized Multiwalled Carbon Nanotubes Using Nitrene Chemistry. *J. Mater. Chem.* **2011**, *21*, 15752−15763.
(20) Mandal, A.; Nandi, A. K. Noncovalent Functionalization of Multiwalled Carbon Nanotube by a Polythiophene-Based Compatibilizer: Reinforcement and Conductivity Improvement in Poly(vinylidene fluoride) Films. *J. Phys. Chem. C* **2012**, *116*, 9360−9371.
(21) Layek, R. K.; Samanta, S.; Chatterjee, D. P.; Nandi, A. K. Physical and Mechanical Properties of Poly (Methyl Methacrylate)-Functionalized Graphene/Poly (Vinylidine Fluoride) Nanocomposites: Piezoelectric β Polymorph Formation. *Polymer* **2010**, *51*, 5846−5856.
(22) Yu, W. X.; Zhao, Z. D.; Zheng, W. T.; Song, Y. M.; Li, B.; Long, B. H.; Jiang, Q. Structural Characteristics of Poly (Vinylidene Fluoride)/Clay Nanocomposites. *Mater. Lett.* **2008**, *62*, 747−750.
(23) Sadeghi, F.; Ajji, A. Study of Crystal Structure of (Polyvinylidene Fluoride/Clay) Nanocomposite Films: Effect of Process Conditions and Clay Type. *Polym. Eng. Sci.* **2009**, *49*, 200−207.
(24) Ramasundaram, S.; Yoon, S.; Kim, K. J.; Park, C. Preferential Formation of Electroactive Crystalline Phases in Poly (Vinylidene Fluoride)/Organically Modified Silicate Nanocomposites. *J. Polym. Sci., Part B* **2008**, *46*, 2173−2187.
(25) Ince-Gunduz, B. S.; Alpern, R.; Amare, D.; Crawford, J.; Dolan, B.; Jones, S.; Kobylarz, R.; Reveley, M.; Cebe, P. Impact of Nanosilicates on Poly (Vinylidene Fluoride) Crystal Polymorphism: Part 1. Melt-Crystallization at High Supercooling. *Polymer* **2010**, *51*, 1485−1493.
(26) Manna, S.; Nandi, A. K. Piezoelectric B Polymorph in Poly (Vinylidene Fluoride)-Functionalized Multiwalled Carbon Nanotube Nanocomposite Films. *J. Phys. Chem. C* **2007**, *111*, 14670−14680.
(27) He, L.; Xu, Q.; Hua, C.; Song, R. Effect of Multiwalled Carbon Nanotubes on Crystallization, Thermal and Mechanical Properties of Poly(Vinylidene Fluoride). *Polym. Compos.* **2010**, 921−927.
(28) Kim, G. H.; Hong, S. M.; Seo, Y. Piezoelectric Properties of Poly (Vinylidene Fluoride) and Carbon Nanotube Blends: B-Phase Development. *Phys. Chem. Chem. Phys.* **2009**, *11*, 10506−10512.
(29) Yu, S.; Zheng, W.; Yu, W.; Jing, Y. Q.; Zhao, Z. Formation Mechanism of β-Phase in PVDF/CNT Composite Prepared by the Sonication Method. *Macromolecules* **2009**, *42*, 8870−8874.
(30) Kim, G. H.; Hong, S. M.; Seo, Y. Piezoelectric Properties of Poly (Vinylidene Fluoride) and Carbon Nanotube Blends: B-Phase Development. *Phys. Chem. Chem. Phys.* **2009**, *11*, 10506−10512.
(31) Mandal, A.; Nandi, A. K. Ionic Liquid Integrated Multiwalled Carbon Nanotube in a Poly (Vinylidene Fluoride) Matrix: Formation of a Piezoelectric B-Polymorph with Significant Reinforcement and Conductivity Improvement. *ACS Appl. Mater. Interfaces* **2013**, *5*, 747−760.
(32) Manna, S.; Batabyal, S. K.; Nandi, A. K. Preparation and Characterization of Silver-Poly (Vinylidene Fluoride) Nanocomposites: Formation of Piezoelectric Polymorph of Poly (Vinylidene Fluoride). *J. Phys. Chem. B* **2006**, *110*, 12318−12326.
(33) Yoon, S.; Prabu, A. A.; Kim, K. J.; Park, C. Metal Salt-Induced Ferroelectric Crystalline Phase in Poly (vinylidene fluoride) Films. *Macromol. Rapid Commun.* **2008**, *29*, 1316−1321.
(34) Wang, F. P.; Lack, A.; Xie, Z. L.; Frubing, P.; Taubert, A.; Gerhard, R. Ionic-Liquid-Induced Ferroelectric Polarization in Poly-(Vinylidene Fluoride) Thin Films. *Appl. Phys. Lett.* **2012**, *100*, 062903.
(35) Xing, C. Y.; Zhao, M. M.; Zhao, L. P.; You, J. C.; Cao, X. J.; Li, Y. J. Ionic Liquid Modified Poly (Vinylidene Fluoride): Crystalline Structures, Miscibility, and Physical Properties. *Polym. Chem.* **2013**, *4*, 5726−5734.
(36) Baji, A.; Mai, Y. W.; Li, Q.; Liu, Y. Electrospinning Induced Ferroelectricity in Poly (Vinylidene Fluoride) Fibers. *Nanoscale* **2011**, *3*, 3068−3071.
(37) Zheng, J.; He, A.; Li, J.; Han, C. C. Polymorphism Control of Poly (Vinylidene Fluoride) Through Electrospinning. *Macromol. Rapid Commun.* **2007**, *28*, 2159−2162.
(38) Andrew, J. S.; Clarke, D. R. Effect of Electrospinning on the Ferroelectric Phase Content of Polyvinylidene Difluoride Fibers. *Langmuir* **2008**, *24*, 670−672.
(39) Yu, L.; Cebe, P. Crystal Polymorphism in Electrospun Composite Nanofibers of Poly (Vinylidene Fluoride) with Nanoclay. *Polymer* **2009**, *50*, 2133−2141.
(40) Andrew, J. S.; Clarke, D. R. Enhanced Ferroelectric Phase Content of Polyvinylidene Difluoride Fibers with the Addition of Magnetic Nanoparticles. *Langmuir* **2008**, *24*, 8435−8438.
(41) Nasir, M.; Matsumoto, H.; Minagawa, M.; Tanioka, A.; Danno, T.; Horibe, H. Formation of B-Phase Crystalline Structure of PVDF Nanofiber by Electrospray Deposition: Additive Effect of Ionic Fluorinated Surfactant. *Polym. J.* **2007**, *39*, 670−674.
(42) Pu, J.; Yan, X.; Jiang, Y.; Chang, C.; Lin, L. Piezoelectric Actuation of Direct-Write Electrospun Fibers. *Sens. Actuators, A* **2010**, *164*, 131−136.

(43) Chang, C.; Tran, V. H.; Wang, J.; Fuh, Y. K.; Lin, L. Direct-Write Piezoelectric Polymeric Nanogenerator with High Energy Conversion Efficiency. *Nano Lett.* **2010**, *10*, 726−731.
(44) Hagiwara, R.; Ito, Y. Room Temperature Ionic Liquids of Alkylimidazolium Cations and Fluoroanions. *J. Fluorine. Chem.* **2000**, *105*, 221−227.
(45) Huddleston, J. G.; Visser, A. E.; Reichert, W. M.; Willauer, H. D.; Broker, G. A.; Rogers, R. D. Characterization and Comparison Of Hydrophilic and Hydrophobic Room Temperature Ionic Liquids Incorporating the Imidazolium Cation. *Green Chem.* **2001**, *3*, 156−164.
(46) Davis, J. H.; Fox, P. A. From Curiosities to Commodities: Ionic Liquids Begin the Transition. *Chem. Commun.* **2003**, 1209−1212.
(47) Wang, P.; Zakeeruddin, S. M.; Exnar, I.; Gratzel, M. High Efficiency Dye-sensitized Nanocrystalline Solar Cells Based on Ionic Liquid Polymer Gel Electrolyte. *Chem. Commun.* **2002**, 2972−2973.
(48) Li, J.; Shen, Y.; Zhang, Y.; Liu, Y. Room-temperature Ionic Liquids as Media to Enhance the Electrochemical Stability of Self-assembled Monolayers of Alkanethiols on Gold Electrodes. *Chem. Commun.* **2005**, 360−362.
(49) Lewandowski, A.; Swiderska, A. Electrochemical Capacitors with Polymer Electrolytes Based on Ionic Liquids. *Solid State Ionics.* **2003**, *161*, 243−249.
(50) Seddon, K. P.; Stark, A.; Torres, M. J. Influence of Chloride, Water, and Organic Solvents on the Physical Properties of Ionic Liquids. *Pure Appl. Chem.* **2000**, *72*, 2275−2287.
(51) Rahman, M.; Brazel, C. S. Ionic Liquids: New Generation Stable Plasticizers for Poly(vinyl chloride). *Polym. Degrad. Stab.* **2006**, *91*, 3371−3382.
(52) Scott, M. P.; Brazel, C. S.; Benton, M. G.; Mays, J. W.; Holbrey, J. D.; Rogers, R. D. Application of Ionic Liquids as Plasticizers for Poly(methyl methacrylate). *Chem. Commun.* **2002**, 1370−1371.
(53) Scott, M. P.; Rahman, M.; Brazel, C. S. Application of Ionic Liquids as Low-volatility Plasticizers for PMMA. *Eur. Polym. J.* **2003**, *39*, 1947−1953.
(54) Bellayer, S.; Gilman, J. W.; Eidelman, N.; Bourbigot, S.; Flambard, X.; Fox, D. M.; Long, H. C.; Trulove, P. C. Preparation of Homogeneously Dispersed Multiwalled Carbon Nanotube/Polystyrene Nanocomposites via Melt Extrusion Using Trialkyl Imidazolium Compatibilizer. *Adv. Funct. Mater.* **2005**, *15*, 910−916.
(55) Fukushima, T.; Kosaka, A.; Yamamoto, Y.; Aimiya, T.; Notazawa, S.; Takigawa, T.; Inabe, T.; Aida, T. Dramatic Effect of Dispersed Carbon Nanotubes on the Mechanical and Electroconductive Properties of Polymers Derived from Ionic Liquids. *Small* **2006**, *2*, 554−560.
(56) Fukushima, T.; Aida, T. Ionic Liquids for Soft Functional Materials with Carbon Nanotubes. *Chem.—Eur. J.* **2007**, *13*, 5048−5058.
(57) Zhao, L. P.; Li, Y. J.; Cao, X. J.; You, J. C.; Dong, W. Y. Multifunctional Role of an Ionic Liquid in Melt-blended Poly(methyl methacrylate)/Multi-walled Carbon Nanotube Nanocomposites. *Nanotechnology* **2012**, *23*, 255702.
(58) Zhao, L. P.; Li, Y. J.; Liu, Z. F.; Shimizu, H. Carbon Nanotube-Conducting Polymer Core−Shell Hybrid Using an Imidazolium-Salt-Based Ionic Liquid As a Linker: Designed As a Potential Platinum Electrode Alternative Material for Large-Scale Solution Processing. *Chem. Mater.* **2010**, *22*, 5949−5956.
(59) Carrion, F. J.; Sanes, J.; Bermudez, M. D.; Arribas, A. New Single-Walled Carbon Nanotubes−Ionic Liquid Lubricant. Application to Polycarbonate−Stainless Steel Sliding Contact. *Tribol Lett.* **2011**, *41*, 199−207.
(60) Xu, H.; Tong, F. F.; Yu, J.; Wen, L. X.; Zhang, J.; He, J. S. A One-pot Method to Prepare Transparent Poly(methyl methacrylate)/Montmorillonite Nanocomposites Using Imidazolium-Based Ionic Liquids. *Polym. Int.* **2012**, *61*, 1382−1388.
(61) Pernak, J.; Czepukowicz, A. New Ionic Liquids and Their Antielectrostatic Properties. *Ind. Eng. Chem. Res.* **2001**, *40*, 2379−2383.
(62) Pernak, J.; Sobaszkiewicz, K.; Foksowicz-Flaczyk, J. Ionic Liquids with Symmetrical Dialkoxymethyl-Substituted Imidazolium Cations. *Chem.—Eur. J.* **2004**, *10*, 3479−3485.
(63) Lu, X. B.; Zhou, J. H.; Zhao, Y. H.; Qiu, Y.; Li, J. H. Room Temperature Ionic Liquid Based Polystyrene Nanofibers with Superhydrophobicity and Conductivity Produced by Electrospinning. *Chem. Mater.* **2008**, *20*, 3420−3424.
(64) Kang, E.; Kim, M.; Oh, J. S.; Park, D. W.; Shim, S. E. Electrospun BMIMPF$_6$/Nylon 6,6 Nanofiber Chemiresistors As Organic Vapour Sensors. *Macromol. Res.* **2012**, *20*, 372−378.
(65) Arumugam, G. K.; Khan, S.; Heiden, P. A. Comparison of the Effects of an Ionic Liquid and Other Salts on the Properties of Electrospun Fibers, 2 − Poly(vinyl alcohol). *Macromol. Mater. Eng.* **2009**, *294*, 45−53.
(66) Seo, J. M.; Arumugam, G. K.; Khan, S.; Heiden, P. A. Comparison of the Effects of an Ionic Liquid and Triethylbenzylammonium Chloride on the Properties of Electrospun Fibers, 1 − Poly(lactic acid). *Macromol. Mater. Eng.* **2009**, *294*, 35−44.
(67) Cheng, W.; Yu, Q.; Qiu, Z.; Yan, Y. Effects of Different Ionic Liquids on the Electrospinning of a Polyacrylonitrile Polymer Solution. *J. Appl. Polym. Sci.* **2013**, *130*, 2359−2368.
(68) Fredlake, C. P.; Crosthwaite, J. M.; Hert, D. G.; Aki, S. N. V. K.; Brennecke, J. F. Thermophysical Properties of Imidazolium-Based Ionic Liquids. *J. Chem. Eng. Data* **2004**, *49*, 954−964.
(69) Xia, Y.; Sasaki, S.; Murakami, T.; Nakano, M.; Shi, L.; Wang, H. Ionic Liquid Lubrication of Electrodeposited Nickel−Si_3N_4 Composite Coatings. *Wear* **2007**, *262*, 765−771.
(70) Huang, W.; Edenzon, K.; Fernandez, L.; Razmpour, S.; Woodburn, J.; Cebe, P. Nanocomposites of Poly(vinylidene fluoride) with Multiwalled Carbon Nanotubes. *J. Appl. Polym. Sci.* **2010**, *115*, 3238−3248.
(71) Liu, Y. L.; Li, Y.; Xu, J. T.; Fan, Z. Q. Cooperative Effect of Electrospinning and Nanoclay on Formation of Polar Crystalline Phases in Poly(vinylidene fluoride). *ACS Appl. Mater. Interfaces* **2010**, *2*, 1759−1768.
(72) Yee, W. A.; Kotaki, M.; Liu, Y.; Lu, X. H. Morphology, Polymorphism Behavior and Molecular Orientation of Electrospun Poly(vinylidene fluoride) Fibers. *Polymer* **2007**, *48*, 512−521.
(73) Gregorio, R.; Cestari, M. Effect of Crystallization Temperature on the Crystalline Phase Content and Morphology of Poly(vinylidene fluoride). *J. Polym. Sci., Part B: Polym. Phys.* **1994**, *32*, 859−870.
(74) Kim, K. J.; Cho, Y. J.; Kim, Y. H. Factors Determining the Formation of the β Crystalline Phase of Poly(vinylidene fluoride) in Poly(vinylidene fluoride)-Poly(methyl methacrylate) Blends. *Vib. Spectrosc.* **1995**, *9*, 147−159.
(75) Benz, M.; Euler, W. B. Determination of the Crystalline Phases of Poly(vinylidene fluoride) Under Different Preparation Conditions Using Differential Scanning Calorimetry and Infrared Spectroscopy. *J. Appl. Polym. Sci.* **2003**, *89*, 1093−1100.
(76) Manna, S.; Nandi, A. K. Piezoelectric β Polymorph in Poly(vinylidene fluoride)-Functionalized Multiwalled Carbon Nanotube Nanocomposite Films. *J. Phys. Chem. C* **2007**, *111*, 14670−14680.
(77) Enomoto, S.; Kawai, Y.; Sugita, M. Infrared spectrum of poly(vinylidene fluoride). *J. Polym. Sci., Part A-2* **1968**, *6*, 861−869.
(78) Wunderlich, B. *Macromolecular Physics: Crystal Melting*; Academic Press: New York, 1980; Vol. 3.
(79) Ko, F.; Gogotsi, Y.; Ali, A.; Naguib, N.; Ye, H.; Yang, G. L.; Li, C.; Willis, P. Electrospinning of Continuous Carbon Nanotube-Filled Nanofiber Yarns. *Adv. Mater.* **2003**, *15*, 1161−1165.